

Chiral Charge-Density Waves

J. Ishioka,¹ Y. H. Liu,² K. Shimatake,¹ T. Kurosawa,² K. Ichimura,^{1,3} Y. Toda,^{1,3} M. Oda,^{2,3} and S. Tanda^{1,3,*}

¹*Department of Applied Physics, Hokkaido University, Sapporo 060-8628, Japan*

²*Department of Physics, Hokkaido University, Sapporo 060-0810, Japan*

³*Center of Education and Research for Topological Science and Technology, Hokkaido University, Sapporo 060-8628, Japan*

(Received 10 January 2010; published 18 October 2010)

We discovered the chirality of charge-density waves (CDW) in $1T$ -TiSe₂ by using STM and time-domain optical polarimetry. We found that the CDW intensity becomes $Ia_1:Ia_2:Ia_3 = 1:0.7 \pm 0.1:0.5 \pm 0.1$, where Ia_i ($i = 1, 2, 3$) is the amplitude of the tunneling current contributed by the CDWs. There were two states, in which the three intensity peaks of the CDW decrease *clockwise* and *anticlockwise*. The chirality in CDW results in the threefold symmetry breaking. Macroscopically, twofold symmetry was indeed observed in optical measurement. We propose the new generalized CDW chirality $H_{\text{CDW}} \equiv \mathbf{q}_1 \cdot (\mathbf{q}_2 \times \mathbf{q}_3)$, where \mathbf{q}_i are the CDW q vectors, which is independent of the symmetry of components. The nonzero H_{CDW} —the triple- q vectors do not exist in an identical plane in the reciprocal space—should induce a real-space chirality in CDW system.

DOI: 10.1103/PhysRevLett.105.176401

PACS numbers: 71.45.Lr, 68.37.Ef, 72.80.Ga, 73.22.Gk

Chirality is an important concept in particle physics and the condensed matter field in relation to baryogenesis [1] or spontaneous symmetry breaking. In condensed matter physics, many researchers have attempted to study the chiral properties of ³He-A [2] and chiral p -wave superconductors [3,4]. Is it possible to break the chiral symmetry in electron systems that also have macroscopic quantum order such as charge-density waves (CDWs)?

Chirality is often characterized by using the parameter of helicity $h = \boldsymbol{\sigma} \cdot \mathbf{p}/|\mathbf{p}|$ ($\boldsymbol{\sigma}$, spin; \mathbf{p} , momentum) in a photon, or $h = \mathbf{v} \cdot \boldsymbol{\omega}$ (\mathbf{v} , velocity; $\boldsymbol{\omega}$, vorticity) in fluids. If the helicity is nonzero in a system, the system has chirality. Chirality describes the character of an object or structure that cannot be superimposed on its mirror image. So far, there is no evidence of the chirality in one-dimensional (1D) CDWs and two-dimensional CDWs, as usual, since a CDW has the form $\rho = \cos(kx + \phi)$ (ρ , charge-density; k , wave number; x , position; ϕ , phase), which is invariant by space inversion, or parity transformation [$k \rightarrow (-k)$ and $x \rightarrow (-x)$].

In this Letter we report the chirality of a CDW in $1T$ -TiSe₂ [5–12] measured directly by using STM and time-domain optical polarimetry. STM is used to investigate the microscopic electron distribution and the phase of the CDW order parameter in real space [5,6,13]. In the measurement, the CDW intensity becomes $Ia_1:Ia_2:Ia_3 = 1:0.7 \pm 0.1:0.5 \pm 0.1$, where Ia_i ($i = 1, 2, 3$) is the amplitude of the tunneling current contributed by the CDWs. We defined a rotation of the phase in terms of the observed CDW intensity differences: *clockwise* and *anticlockwise*. Two chiral phases were observed. Moreover, the two-color pump-probe pulse method was performed to determine the macroscopic property by changing the linearly polarized angle of the probe pulse. A twofold property in transient reflectivity was detected. To explain these results, we propose a new CDWs configuration based on the 3D

CDW q vectors of $1T$ -TiSe₂ in reciprocal space. In real space, the relative phase shifts between three CDW q vectors induce the helical structure in CDW unit cells. We provide the first evidence of chirality in a CDW. Moreover, we propose generalized CDW chirality in triple- q systems as $H_{\text{CDW}} \equiv \mathbf{q}_1 \cdot (\mathbf{q}_2 \times \mathbf{q}_3)$.

$1T$ -TiSe₂ crystallizes in a $1T$ -CdI₂-type structure. The crystal is constructed of Se-Ti-Se layers. All the Se-Ti-Se layers are weakly accumulated by the van der Waals attraction along the c axis. $1T$ -TiSe₂ undergoes a CDW transition into a $2a_0 \times 2a_0 \times 2c_0$ superlattice ($a_0 = 3.54 \text{ \AA}$, $c_0 = 6.00 \text{ \AA}$ are lattice constants) at $T_c = 200 \text{ K}$ [10].

We synthesized a single crystal of $1T$ -TiSe₂ using the self-vapor transportation method [7]. By controlling the growth temperature, we obtained sample *A* at $700 \text{ }^\circ\text{C}$ and sample *B* at $800 \text{ }^\circ\text{C}$. The resistivity behavior of each sample was consistent with that described in the previous report [8,14].

In the STM measurements, the samples were cleaved *in situ* just before the approach of the STM tip toward the surface in an ultrahigh vacuum at 77 K . We were able to observe atomically resolved STM images in the constant height mode with a constant sample voltage V_s applied between the tip and the sample. The STM images of samples *A* and *B* were obtained at 84 and 6.3 K , respectively.

The two-color pump-probe pulse method [15–17] was employed with the cleaved TiSe₂ surface using a micro-optical setup as mentioned in Ref. [18]. The pump and probe pulse polarization was varied to investigate the dominant direction of the deviation of reflectivity $\Delta R(t)$. The sample was measured at 3 K .

Figures 1(a) and 1(b) show STM images and line profiles along unit vectors, respectively. Figure 1 shows the low symmetry structure of the electron distribution in TiSe₂ with atomic resolution in sample *A*. In Fig. 1(a), the bright

area is the point at which many electrons are tunneling. We observed a triangular lattice of Se atoms with a lattice constant a_0 . In addition, we saw a $2a_0$ wavelength CDW along the unit vectors. To compare the amplitude of the CDW intensity for each CDW q direction, we show the line profiles of the tunneling currents along the unit vectors \mathbf{a}_1 , \mathbf{a}_2 , and \mathbf{a}_3 [Fig. 1(b)]. In Fig. 1(b), there is obvious difference in CDW amplitude among each direction of the unit vector. The CDW amplitude I_{ai} was specified for each magnitude and labeled in order starting with the largest amplitude. In sample A, $I_{a1}:I_{a2}:I_{a3} = 1:0.7:0.5$. This STM image does not have the threefold symmetry owing to a triangular lattice structure. In general, the line profiles consist of the sum of two of the three density waves [Fig. 1(a)]. It is necessary to separate the contribution of each CDW.

Figures 1(c) and 1(d) show a Fourier transformation (FT) image of sample A and line profiles along the CDW q vectors, respectively. In Fig. 1(c), the bright spots correspond to the intensity peak of each wave vector. The outer intensity peaks are the Bragg peaks of the selenium lattice whose wavelength is a_0 . The inner peaks correspond to a CDW satellite whose wavelength is $2a_0$. In Fig. 1(d), there is no difference in the intensity of Bragg peaks which correspond to each \mathbf{a}^* vector, where \mathbf{a}^* is a basis of reciprocal lattice. In contrast, we can see an obvious difference between the three sets of CDW intensity peaks. Then, we denote the wave vectors \mathbf{q}_1 , \mathbf{q}_2 , and \mathbf{q}_3 in order starting with the highest intensity, too [Fig. 1(d)]. In sample A, $I_{q1}:I_{q2}:I_{q3} = 1:0.9:0.5$. In terms of the rotation in which the indexed number increases [inset in Fig. 1(c)],

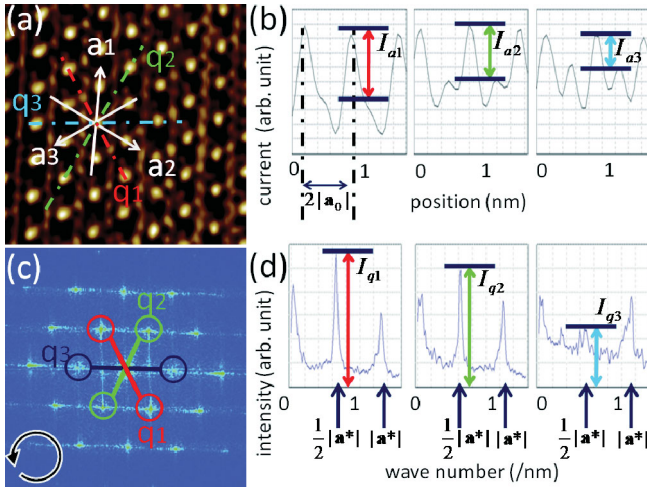


FIG. 1 (color). (a) $3.5 \text{ nm} \times 3.5 \text{ nm}$ STM images and (b) line profiles along unit vector \mathbf{a}_1 , \mathbf{a}_2 , and \mathbf{a}_3 . I_{ai} is the amplitude of the line profiles along \mathbf{a}_i . Sample A was cleaved in 10^{-8} Torr at 77 K and measured *in situ* at a sample bias voltage of $V_s = 150 \text{ mV}$ and an initial tunneling current of $I_t = 0.3 \text{ nA}$ at $T = 84 \text{ K}$. (c) FT image of sample A and (d) line profiles along \mathbf{q}_1 , \mathbf{q}_2 , \mathbf{q}_3 wave vector. I_{qi} is the intensity of the line profiles along \mathbf{q}_i . FT was performed over the entire field of view ($25 \text{ nm} \times 25 \text{ nm}$) of STM image.

we name the phase the anticlockwise phase. In further STM experiment, we also found a clockwise phase in the same sample.

Figure 2(a) shows $12 \text{ nm} \times 12 \text{ nm}$ STM images in sample B, and Figs. 2(b) and 2(c) show the FT of two areas each enclosed with a square. In Fig. 2(a), the clockwise and anticlockwise phases were observed simultaneously. Figure 2(b) is clockwise and Fig. 2(c) is anticlockwise phase; that is, Fig. 2(b) is a mirror image of Fig. 2(c). Therefore, Fig. 2(b) cannot be superimposed on Fig. 2(c) solely with rotational transformation. Thus, the results show the parity symmetry breaking. Although Slough *et al.* [5] and Coleman *et al.* [6] observed anisotropy in the conductive plane in a previous STM measurement, the mirror image relation was not demonstrated within their analysis by contour plotting. We discovered two phases with different chirality. The blue line in Fig. 2(a) shows the boundary between the clockwise and anticlockwise phases. Because we found no steps of atomic layer and no changes of the lattice direction, this is not a crystallographic defect in the observed layer. Thus, the boundary between the two phases is a chiral domain wall.

Figures 3(a) and 3(b) show the polarization dependence of the transient reflectivity variation of a 700°C grown $1T\text{-TiSe}_2$ measured at 3 K and $1T\text{-TaS}_2$ measured at 12 K, respectively. Figure 3 shows the clear twofold symmetry in TiSe_2 . The transient variation in optical reflectance $\Delta R(t)$ was measured by changing the polarization angle E_{pol} of the incident probe laser pulse. In general, the peak intensity of transient signals corresponds to the number of electrons excited over the CDW gap [19,20]. But in Fig. 3(a), the peak intensity behaved anisotropically. Surprisingly, when we plot the peak intensity as a function of polarization angle E_{pol} [Fig. 3(c)], we observed twofold symmetry although $1T\text{-TiSe}_2$ has a trigonal lattice structure. In con-

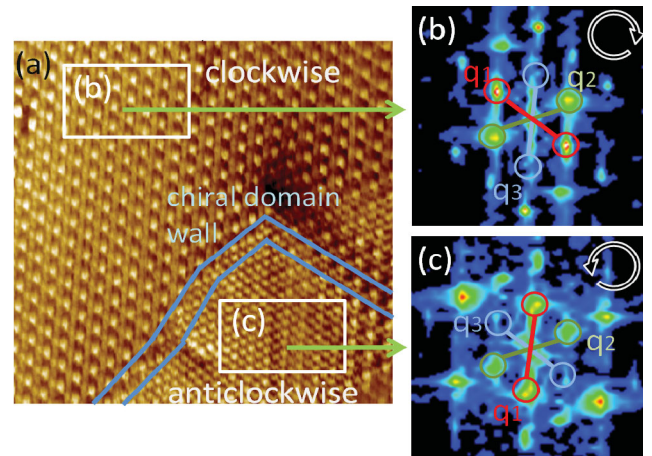


FIG. 2 (color). (a) $12 \text{ nm} \times 12 \text{ nm}$ STM image and (b),(c) FT of two areas each enclosed with a square in sample B. Sample B was measured at $V_s = -350 \text{ mV}$ and $I_t = 0.4 \text{ nA}$ at $T = 6.3 \text{ K}$. The blue line is the domain wall between the clockwise phase and the anticlockwise phase.

trast, this clear twofold property is not seen with $1T$ -TaS₂, which is the most common 2D CDW material with the same lattice structure [Figs. 3(b) and 3(d)]. In general, the twofold symmetry does not emerge solely in most two-dimensional CDW systems because three CDWs generate a triangular lattice that has threefold and twofold symmetry simultaneously. Thus, at least within the light penetration length, a spatial twofold structure was achieved in the CDW system. The macroscopic twofold property is consistent with the microscopic twofold symmetry observed with STM as shown in Fig. 1(b).

To understand these results, let us consider the static charge distribution in real space. We propose a simple model of the CDW stacking. The CDW stacking is not conventional layer stacking with 2D CDW sheets [21–23] but CDW component stacking that makes internal structure in a CDW unit cell. Figure 4 shows the configuration of three CDW components. Charge concentration is indicated by the deeply colored part. Each color corresponds to the CDW q vector illustrated in the inset of Fig. 4. When we consider the charge-density corresponding to the wave vector \mathbf{q}_i ($i = 1, 2, 3$), $\rho_{q_i} = A \cos(\mathbf{q}_i \cdot \mathbf{r} + \phi_i)$, where A is the amplitude and ϕ_i is the initial phase. In our model, we considered relative phase shift between each CDW. In the TiSe₂ system, the wave vector \mathbf{q}_i have \mathbf{c}^* component which corresponds to the $2c_0$ periodicity. We assumed $\phi_1 = 0$, $\phi_2 = 2\pi/3$, and $\phi_3 = 4\pi/3$. This assumption leads to the CDW density peak shift along the c direction at the interval of $2c_0/3$. The shifted density peaks exist in *virtual* layers which are indicated as the dotted lines in

Figs. 4(a) and 4(b). Chirality is achieved by twisted stacking such as with cholesteric liquid crystals [24]. Thus, CDW component stacking results in *helical* stacking and helical axis parallel to the c axis. Note that by putting three density peaks in $2c_0$, there are two ways of CDW stacking; that is, when we permute the sequence of two colored density waves (blue and green), the helix is inverted [Fig. 4(a)]. A charge helix along the c axis was achieved in the CDWs, and the helicity difference results from the stacking sequence.

This configuration can explain the low symmetry charge distribution in the STM measurement and the twofold symmetry in the optical measurement. In the STM measurement, the tunneling current can obtain information about one or two atomic layers. In one atomic layer, the intensity of three CDWs differs due to the distance between the observed surface and each CDW peak. A CDW whose peak was closer to the surface was more clearly observed (Iq_1) than a CDW that was further away (Iq_3). This difference breaks the threefold symmetry. Let us consider the CDW layers depicted as red and blue layer in our model. The CDW distribution forms twofold symmetry in the red layer and the CDW also forms twofold symmetry in the blue layer. Consequently, the whole layers form twofold symmetry of the system since the optical measurement reflects the superposition of all of the layers. In terms of the intensity difference between Iq_1 and Iq_3 , the FT image obtained with STM (Fig. 2) reveals the direction of the helical stacking. Clockwise is the “left-handed” and anti-clockwise is the “right-handed” state.

To consider the origin of the helical stacking of CDW, we take account of the each q vector with a \mathbf{c}^* component in $1T$ -TiSe₂ [9] unlike those in $1T$ -TaS₂. In typical 2D CDW materials, such as $1T$ -TaS₂, at first the in-plane triple- q vectors form a hexagonal superlattice structure in a S-Ta-S layer. Then, by the Coulomb interaction, the S-Ta-S layers stack with the next CDW layer so as no two density peaks have the same position [Fig. 4(c)]. We call this conventional layer stacking. The phase shift in the neighboring layer results from interlayer coupling. On the other hand, in $1T$ -TiSe₂, the 3D q vectors, that originally have a c -axis component, induce a charge modulation directly along the q vectors. Accordingly, in $1T$ -TiSe₂ there is no such conventional layer stacking. Moreover, relative phase shifting along the c axis between \mathbf{q}_1 , \mathbf{q}_2 , and \mathbf{q}_3 can reduce the Coulomb interaction. As a result, the configuration achieves a helical structure (Fig. 4). Moreover, since there are three q vectors, CDWs can form two types of helical stacking based on the stacking sequence: clockwise and anticlockwise. Therefore, three-dimensional triple q vectors make chirality in CDW systems.

From the above discussion, we propose generalized CDW chirality in triple q in reciprocal space:

$$H_{\text{CDW}} \equiv \mathbf{q}_1 \cdot (\mathbf{q}_2 \times \mathbf{q}_3), \quad (1)$$

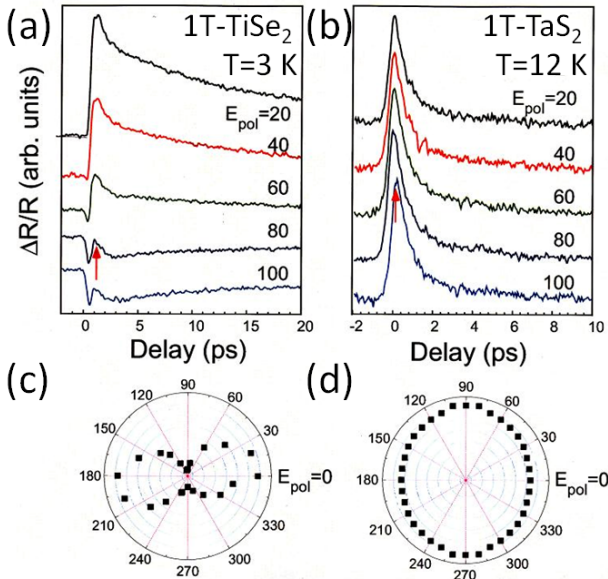


FIG. 3 (color online). Polarization dependence of transient reflectivity variation in $1T$ -TiSe₂ measured at 3 K (a) and $1T$ -TaS₂ measured at 12 K (b). The height of each peak is plotted in the (c) and (d) as function of polarization angle E_{pol} . The pump pulse wavelength is 1160 nm and the power is 150 μW . The probe pulse is 800 nm, 80 μW .

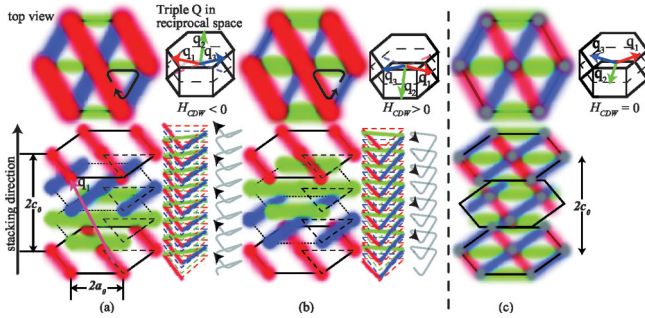


FIG. 4 (color). Schematic representation of (a) left-handed chiral CDWs and (b) right-handed chiral CDWs in a TiSe_2 CDW unit cell in real space and (c) typical 2D CDW. Charge concentration is indicated by the deeply colored part. The colors correspond to the colored CDW q vector in the inset. In a CDW unit cell, the density peaks of three CDW are shifted at intervals of $2c_0/3$. If we look at one layer, the different intensities of three CDWs form a low symmetry structure. There are two phases caused by difference in stacking direction (red-blue-green or red-green-blue). As with cholesteric liquid crystals, the stacking results in the helicity of CDW systems. There is a mirror-image relation between the two configurations in (a) and (b). As well as the stacking of CDWs layers in real space, CDW helicity defined in reciprocal space, $H_{\text{CDW}} \equiv \mathbf{q}_1 \cdot (\mathbf{q}_2 \times \mathbf{q}_3)$, reverses by space inversion [$\mathbf{q}_i \rightarrow (-\mathbf{q}_i)$]. H_{CDW} is positive in a right-handed chiral CDW, and H_{CDW} is negative in a left-handed chiral CDW.

where \mathbf{q}_1 , \mathbf{q}_2 , and \mathbf{q}_3 are the CDW q vectors. If the H_{CDW} is zero (three CDW q vectors in one atomic plane), a triple- q CDW exists simultaneously in one layer in a CDW unit cell. But if the H_{CDW} is nonzero (inset in Fig. 4), there is a degree of freedom owing to charge helicity; that is, $H_{\text{CDW}} < 0$ represents a left-handed chiral CDW and $H_{\text{CDW}} > 0$ represents a right-handed chiral CDW. The space inversion of three q axes inverts the sign of H_{CDW} (right-handed to left-handed) (Fig. 4). Therefore, we predict that there will be CDW component stacking in a CDW system where $H_{\text{CDW}} \neq 0$ and therefore the CDWs themselves will have chirality.

Finally, we briefly discuss the phase transition in TiSe_2 . Originally, TiSe_2 is a mystery because the Fermi surface nesting scenario cannot explain all of the phase transition [11,12]. Based on our discovery, we can suggest a new scenario about the unconventional phase transition considering the chiral phases. That is, the anomalously broad peak with a width of 100 K in the resistivity in the phase transition [8] may be a consequence of the frustration of left-handed and right-handed phases separated by chiral domain walls. A domain wall, which is a boundary between the superlattices, will behave as a conductive path. Therefore, chiral CDW will not have sharp resistivity peaks. Moreover, it is interesting that the CDW system in which the wave function is generally based on the s -wave symmetry has the chirality such as cholesteric liquid crystals despite no isotropic component. Our discovery sheds new light on the old and rather controversial problem of CDW instability and opens the possibility to explore di-

rectly the interplay between chirality and transport in electron systems. Our findings could also pave the way towards the investigation of charge helicity and external fields.

We thank K. Yamaya and T. Toshima for providing advice on sample preparation. We also thank K. Inagaki, T. Matsuura, and H. Nobukane for measuring the electrical property and for fruitful discussions. And we thank N. Hatakenaka for helpful comments. This work was supported by the 21COE program on ‘‘Topological Science and Technology’’ from Ministry of Education, Culture, Science and Technology of Japan.

*Corresponding author.

tanda@eng.hokudai.ac.jp

- [1] A. D. Dolgov, *Phys. Rep.* **222**, 309 (1992).
- [2] G. E. Volovik, *Exotic Properties of Superfluid ^3He* (World Scientific, Singapore, 1992).
- [3] A. P. Mackenzie and Y. Maeno, *Rev. Mod. Phys.* **75**, 657 (2003).
- [4] H. Nobukane *et al.*, *Solid State Commun.* **149**, 1212 (2009).
- [5] C. G. Slough *et al.*, *Phys. Rev. B* **37**, 6571 (1988).
- [6] R. V. Coleman *et al.*, *Adv. Phys.* **37**, 559 (1988).
- [7] I. Taguchi *et al.*, *Physica (Amsterdam)* **105B**, 146 (1981).
- [8] F. J. DiSalvo, D. E. Moncton, and J. V. Waszczak, *Phys. Rev. B* **14**, 4321 (1976).
- [9] A. Zunger and A. J. Freeman, *Phys. Rev. B* **17**, 1839 (1978).
- [10] K. C. Woo *et al.*, *Phys. Rev. B* **14**, 3242 (1976).
- [11] J. A. Wilson, *Solid State Commun.* **22**, 551 (1977).
- [12] T. E. Kidd *et al.*, *Phys. Rev. Lett.* **88**, 226402 (2002).
- [13] Z. Z. Wang *et al.*, *Phys. Rev. B* **67**, 121401 (2003).
- [14] T_c of the samples decrease with higher growth temperature: T_c of sample A and B are 198 and 185 K, respectively. The maximum resistance of sample A at 145 K is 5.5 times as large as that in room temperature. And that of sample B at 160 K is 1.4 times as large as that. A systematic study for impurity effect is reported in E. Morosan *et al.*, *Nature Phys.* **2**, 544 (2006).
- [15] G. Li *et al.*, *Phys. Rev. Lett.* **99**, 027404 (2007).
- [16] K. Rosnagel, L. Kipp, and M. Skibowski, *Phys. Rev. B* **65**, 235101 (2002).
- [17] Y. Miyahara *et al.*, *J. Phys. Condens. Matter* **7**, 2553 (1995).
- [18] K. Shimatake, Y. Toda, and S. Tanda, *Phys. Rev. B* **75**, 115120 (2007).
- [19] J. Demsar, K. Biljaković, and D. Mihailovic, *Phys. Rev. Lett.* **83**, 800 (1999).
- [20] J. Demsar, L. Forró, H. Berger, and D. Mihailovic, *Phys. Rev. B* **66**, 041101 (2002).
- [21] S. Tanda, T. Sambongi, T. Tani, and S. Tanaka, *J. Phys. Soc. Jpn.* **53**, 476 (1984).
- [22] S. Tanda and T. Sambongi, *Synth. Met.* **11**, 85 (1985).
- [23] K. Nakanishi and H. Shiba, *J. Phys. Soc. Jpn.* **53**, 1103 (1984).
- [24] P. M. Chaikin and T. C. Lubensky, *Principles of Condensed Matter Physics* (Cambridge University Press, London, 1995).